Co-Induced Electronic Optimization of Hierarchical NiFe LDH for Oxygen Evolution

Yanping Lin, Hao Wang, Chun-Kuo Peng, Liangmin Bu, Chao-Lung Chiang, Kai Tian, Yue Zhao, Jianqing Zhao,* Yan-Gu Lin, Jong-Min Lee,* and Lijun Gao*

Developing efficient and stable non-noble electrocatalysts for the oxygen evolution reaction (OER) remains challenging for practical applications. While nickel–iron layered double hydroxides (NiFe-LDH) are emerging as prominent candidates with promising OER activity, their catalytic performance is still restricted by the limited active sites, poor conductivity and durability. Herein, hierarchical nickel–iron–cobalt LDH nanosheets/carbon fibers (NiFeCo-LDH/CF) are synthesized through solvent-thermal treatment of ZIF-67/CF. Extended X-ray adsorption fine structure analyses reveal that the Co substitution can stabilize the Fe local coordination environment and facilitate the π-symmetry bonding orbital in NiFeCo-LDH/CF, thus modifying the electronic structures. Coupling with the structural advantages, including the largely exposed active surface sites and facilitated charge transfer pathway ensured by CF, the resultant NiFeCo-LDH/CF exhibits excellent OER activity with an overpotential of 249 mV at 10 mA cm^{-1} as well as robust stability over 20 h.

1. Introduction

The fast-growing demand for energy and rapid consumption of fossil fuels have forced people to develop renewable, sustainable, and clean energy sources.[1] Oxygen evolution reaction (OER) plays a key role in renewable energy technology, such as electrochemical water splitting and fuel cells. However, the sluggish kinetics of electrocatalysts in OER (a complicated four-electron transfer reaction) limit their performance and wide use in such two areas.[2,3] In this regard, highly efficient and

sturdy oxygen evolution electrocatalysts are demanded to lower the high reaction overpotential (η) and accelerate reaction dynamics. So far, noble metal based materials, such as IrO_2 and RuO_2, are known as the most efficient OER catalysts in alkaline environment.[2,3] Nevertheless, the large-scale application of Ir and Ru based catalysts in industrial production is severely hindered by their deficiency and high cost. To settle this problem, a great deal of non-noble metal-based catalysts, for example, perovskite oxides,[4] transition-metal oxides,[5] nitrides,[6] carbides,[7] sulfides,[8] and (oxy)hydroxides[9] have been widely explored to facilitate the reaction rate of OER in electrocatalytic water splitting.

Among reported non-noble metal-based OER catalysts, transition-metals (Fe, Co, Ni, and Mn) oxides/hydroxides have triggered enormous interests. In particular, NiFe-LDHs have attracted significant attention owing to the prominent OER electrocatalytic property in alkaline solutions.[9a,e,10] Boettcher and co-workers[11] suggested that the intensive FeIII can adjust the valence state of NiII in Ni(OH)$_2$ and NiIII in NiOOH during the electrochemical reaction process and thus promote the electrocatalytic performance. However, further activity promotion for NiFe-LDHs is still an enormous challenge due to their restricted active sites, poor electrical conductivity and durability. Previous studies have demonstrated that appropriate structuring could increase the active surface area and facilitate charge transfer of the catalysts, delivering enhanced electrocatalytic performance[8a,9b,c,12]

Zeolitic imidazolate frameworks (ZIFs), a class of famous metal–organic frameworks, have been diffusely applied as both a kind of templates and metal source in the fabrication of energy storage and conversion materials.[13] In particular, ZIF-67 combined with cobalt ion and dimethylimidazole can be easily dissolved in acidic condition.[14] Meanwhile, cobalt ion can supply trivalent ions to the LDH materials owing to their alterable valences.[15] Beside, the incorporation of another metal can tune the electronic structure in the NiFe-LDH material, contributing to the improved intrinsic catalystic activity.[16] Hence, it would be easy to assume that ZIF-67 can be used as a third metal source as well as surfactant-like to adjust the composition and optimize the morphology of NiFe-LDH. Furthermore, the poor conductivity of metal oxides/hydroxides can be improved by bonding carbon materials, especially variety of

Y. Lin, L. Bu, K. Tian, Y. Zhao, Prof. J. Zhao, Prof. L. Gao
College of Energy
Soochow Institute for Energy and Materials Innovations
& Key Laboratory of Advanced Carbon Materials and Wearable Energy
Technologies of Jiangsu Province
Soochow University
Suzhou 215006, China
E-mail: jqzhao@suda.edu.cn; gaolijun@suda.edu.cn
Dr. H. Wang, Prof. J.-M. Lee
School of Chemical and Biomedical Engineering
Nanyang Technological University
Singapore 637459, Singapore
E-mail: jmlee@ntu.edu.sg
C.-K. Peng, Dr. C.-L. Chiang, Dr. Y. Lin
National Synchrotron Radiation Research Center
Hsinchu, Taiwan 30076, R.O.C.

ADVANCED
SCIENCE NEWS
www.advancedsciencenews.com

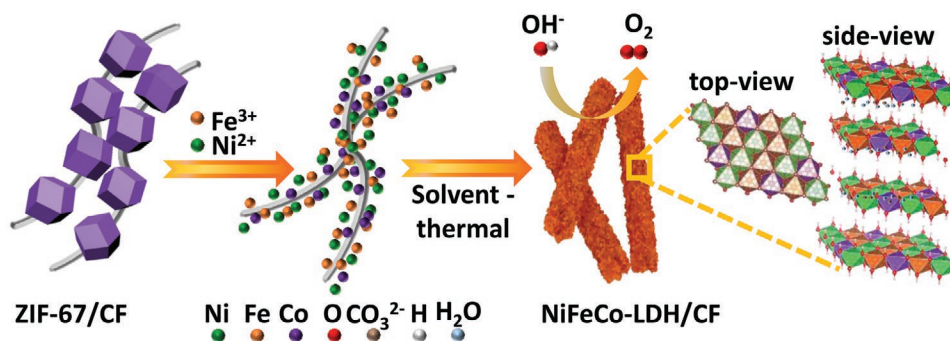NANO · MICRO
small
www.small-journal.com

Figure 1. Schematic illustration of synthetic procedure of NiFeCo-LDH/CF electrocatalyst for OER.

carbon nanotubes constituted with interconnected electrically conducting network.[17]

Herein, we report on a novel strategy to fabricate a hierarchically structured NiFeCo-LDH/CF composite by sacrificing ZIF-67 grown on carbon fiber (ZIF-67/CF) as the cobalt source and surfactant-like and in situ coprecipitating multimetal cations. The frizzy ultrathin nanosheets of NiFeCo-LDH growing on carbon fiber could completely expose its active sites by diminishing the thickness and increasing the specific surface area. In addition, the sufficient supply of electron for NiFeCo-LDH/CF could be ensured with the conductively tubular frizzy structure established by CF during the electrocatalytic OER process. The Co substitution can stabilize the Fe local coordination environment and facilitate the π-symmetry bonding orbital in NiFeCo-LDH/CF, thus modifying the electronic structures and improving the OER activity. In consequence, the electrocatalytic activity of NiFeCo-LDH/CF for OER could be enhanced with an overpotential of 249 mV at current density of 10 mA cm^{-2} and robust stability over 20 h.

2. Results and Discussion

The general strategy to synthesize NiFeCo-LDH/CF is schematically illustrated in **Figure 1**. First, uniform ZIF-67/CF was prepared via a room-temperature method, which was similar with the preparation of ZIF-67,[12a] except the incorporation of untreated commercial CF with a diameter of around 30 nm (Figure S2, Supporting Information). The rhombic dodecahedrons ZIF-67 were grown across the carbon fiber with an average particle size of 300 nm (Figure S3, Supporting Information). Subsequently, ZIF-67/CF was dispersed into an isopropanol/glycol mixture solvent. Following with the addition of nickel and iron nitrate, ZIF-67 was etched, releasing Co^{2+}, due to the acidic environment triggered by the high hydrolysis of Ni^{2+} and Fe^{3+}. At the same time, the three metal cations coprecipitated homogeneously on CF to form NiFeCo-LDH,[15] which can be evidenced by the scanning electron microscope (SEM) images of the intermediate in Figure S4 of the Supporting Information. Finally, after the solvent thermal treatment, NiFeCo-LDH/CF with tubular frizzy nanosheets structure was successfully synthesized. An optimal relative composition was essential to achieve an ideal structure, which was derived as NiFeCo-LDH/CF(0.075) by using ZIF-67/CF with CF content of 7.5% as the precursor (Figures S5, Supporting Information).

For comparison, NiFeCo-LDH without CF was also prepared by using the ZIF-67 as surfactant-like and cobalt source, which shows bulk structure with an average size of 200 nm accompany with less nanosheets. (Figure S6, Supporting Information).

The detailed morphological characterizations of NiFeCo-LDH/CF are displayed in **Figure 2**. The SEM and transmission electron microscopy (TEM) images show that a mass of frizzy NiFeCo-LDH nanosheets are homogeneously cross-stacked on CF with a total diameter of 300 nm (Figure 2a,b). Notably, this edge-rich NiFeCo-LDH/CF could expose larger surface area than the conglobate bulk morphology of NiFe-LDH (Figure S7, Supporting Information). Besides, it is interesting to find that the largely tubular frizzy nanosheets structure with thickness of 3.5–4.9 nm relied on the CF support. However, NiFeCo-LDH synthesized without CF exhibited a much larger particle size and tended to aggregate into bulk. The incorporation of CF can effectively prevent the ultrathin nanosheets from aggregation. Such an open nanostructure of NiFeCo-LDH ultrathin nanosheets could increase the density of electrochemical active sites and the accessibility of electrolyte, thus promoting OER activity of the electrocatalyst.[18] The high-resolution transmission electron microscopy (HRTEM) image in Figure 2c further discloses a clear hierarchical structure of NiFeCo-LDH/CF. Besides, it also shows that the NiFeCo-LDH is tightly coupled with CF. Such structural advantage can facilitate charge transport pathway, thus improving the OER property. The selected-area electron diffraction (SAED) pattern (inset in Figure 2c) displays that the NiFeCo-LDH/CF has two diffraction rings belong to NiFe-LDH. Furthermore, the atomic-resolution TEM image (Figure 2d) reveals obvious lattice fringes with an interplanar spacing of 2.57 Å, which is corresponded to the (012) plane of NiFe-LDH. Inductively coupled plasma optical emission spectrometry revealed a mole ratio of 1.05:1:0.38 and atomic ratio of 43.21%, 41.1%, and 15.96% for Ni/Fe/Co in NiFeCo-LDH/CF (Table S1, Supporting Information). The high angle annular dark-field (HAADF) image and elemental mapping images (Figure 2e,f) indicate that Ni, Fe, and Co elements are uniformly dispersed over the sample.

XRD measurement was carried out to confirm the crystallography characteristic of the as-prepared pure NiFeCo-LDH/CF, NiFeCo-LDH, and NiFe-LDH. As shown in **Figure 3**a, for NiFe-LDH, reflections at $2\theta = 10.3°$, $21.7°$, $34.5°$, and $60.7°$ can be indexed as (003), (006), (012), and (110) diffraction peaks of NiFe-LDH (JCPDS 51-0463), respectively.[17b,19] Meanwhile, the XRD patterns of NiFeCo-LDH and NiFeCo-LDH/CF could
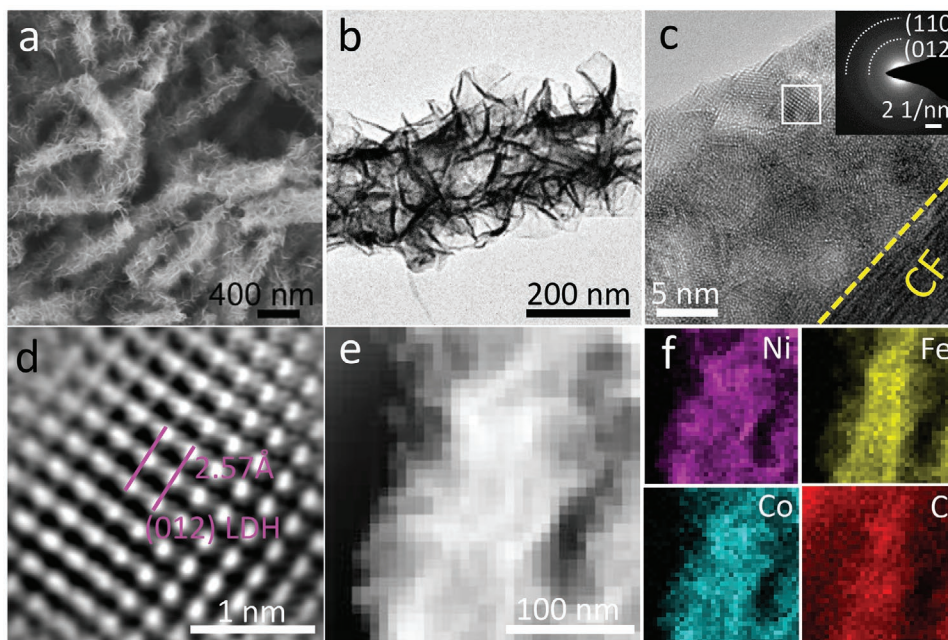
Figure 2. a) SEM and b) TEM image of NiFeCo-LDH/CF. c) HRTEM image and d) atomic-resolution TEM image of NiFeCo-LDH/CF. The upper right inset of (c) is the corresponding SAED pattern. e) HAADF-STEM image and f) corresponding EDS elemental mapping images of NiFeCo-LDH/CF.

match well with that of NiFe-LDH, indicating that the LDHs were well-crystallized and the Co doping did not cause any structure transformation in the two samples. The diffraction peak of (003) facet at 10.3° was associated with an interlayer separation of 0.77 nm, manifesting that CO_3^{2-} and H_2O occupied the LDH interlayer channel, which can be demonstrated by the FT-IR spectra in Figure 3b. A broad absorption located at 3420 cm^{-1} is assigned to the O—H stretching of interlayer water molecules and the obvious peak at 1630 cm^{-1} can be assigned to the bending vibration of interlayer H_2O.[20] The absorption peaks at ≈680 and ≈510 cm^{-1} are attributed to the vibrations of metal–O and metal–O–metal bonds, respectively.[21] Additionally, there are no characteristic stretching vibration of C—N and bending vibration of imidazole ring for dimethylimidazole in NiFeCo-LDH and NiFeCo-LDH/CF, indicating the absence of dimethylimidazole in the two samples. To evaluate the specific surface area and permanent porosity of the catalysts, nitrogen adsorption/desorption was carried out and the corresponding isotherms and pore size distribution of the as prepared materials are presented in Figure 3c. In comparison to NiFe-LDH in Type I isotherm (representative of microporous materials), the shape of the isotherm for NiFeCo-LDH/CF and NiFeCo-LDH can be classified as the type IV isotherm, therefore standing for mesoporous materials. The specific surface area of NiFeCo-LDH/CF and NiFeCo-LDH were calculated to be 225 and 116 m^2 g^{-1} using the Brunauer–Emmett–Teller method, respectively, which are larger than that of NiFe-LDH (71 m^2 g^{-1}). The introduction of CF effectively prevents the ultrathin nanosheets from aggregation, thus endowing NiFeCo-LDH/CF an open nanostructure with larger specific surface area, which could be in favor of OER. Based on the BJH calculation, two distinct peaks related to the pore width of 3.85 and 3.9 nm for NiFeCo-LDH/CF and NiFeCo-LDH, respectively, are observed

in Figure 3d. It is commonly recognized that the internal large with a mass of mesopores can create a more exoteric structure which is conducive to the mass transfer, hence improving OER performance of the catalyst.[22]

XPS was applied to better understand the electronic interaction and charge transfer between Fe/Co and Ni at the surface of the as-synthesized catalysts. The XPS spectra in Figure S8 of the Supporting Information demonstrate the presence of Ni, Fe, and Co in the samples of NiFeCo-LDH and NiFeCo-LDH/CF, whereas the Co signal is absent in NiFe-LDH. For NiFeCo-LDH/CF, the Ni 2p spectrum shown in **Figure 4**a exhibits two fitting peaks at 872.9 and 855.2 eV combined with two satellites at 879.2 and 861.1 eV, which are associated with Ni^{2+}.[23] In the high-resolution XPS spectra of Fe 2p (Figure 4b), two distinct peaks of Fe $2p_{1/2}$ and Fe $2p_{3/2}$ appearing at 724.7 and 711.2 eV reveal the existence of Fe^{3+} in the three samples.[10h] It is worth noting that the binding energy of Ni 2p and Fe 2p for Co doped ternary materials (NiFeCo-LDH and NiFeCo-LDH/CF) shifted evidently to higher binding energy compared to that of NiFe-LDH, which indicates a strong electronic interaction between Co and NiFe-LDH. The Co $2p_{1/2}$ and Co $2p_{3/2}$ peaks in Figure 4c can be deconvoluted into four peaks locating at 797.0/782.3 eV (Co^{2+}) and 796.0/780.1 eV (Co^{3+}), respectively, indicating that the Co atom is basically in the valence state of +2 and +3 in NiFeCo-LDH/CF.[12a] Moreover, after the combination of CF, the Co 2p peaks for NiFeCo-LDH/CF shift to positive binding energy (+0.5 eV), demonstrating the existence of electron transport between NiFeCo-LDH and CF within NiFeCo-LDH/CF.

The local electronic structures and atomic arrangements of the as-synthesized catalysts were investigated by X-ray absorption near-edge structure (XANES) and extended X-ray absorption fine structure (EXAFS) spectra. The edge-jumps of Fe, Co, and Ni elements in the XANES spectra were attributed
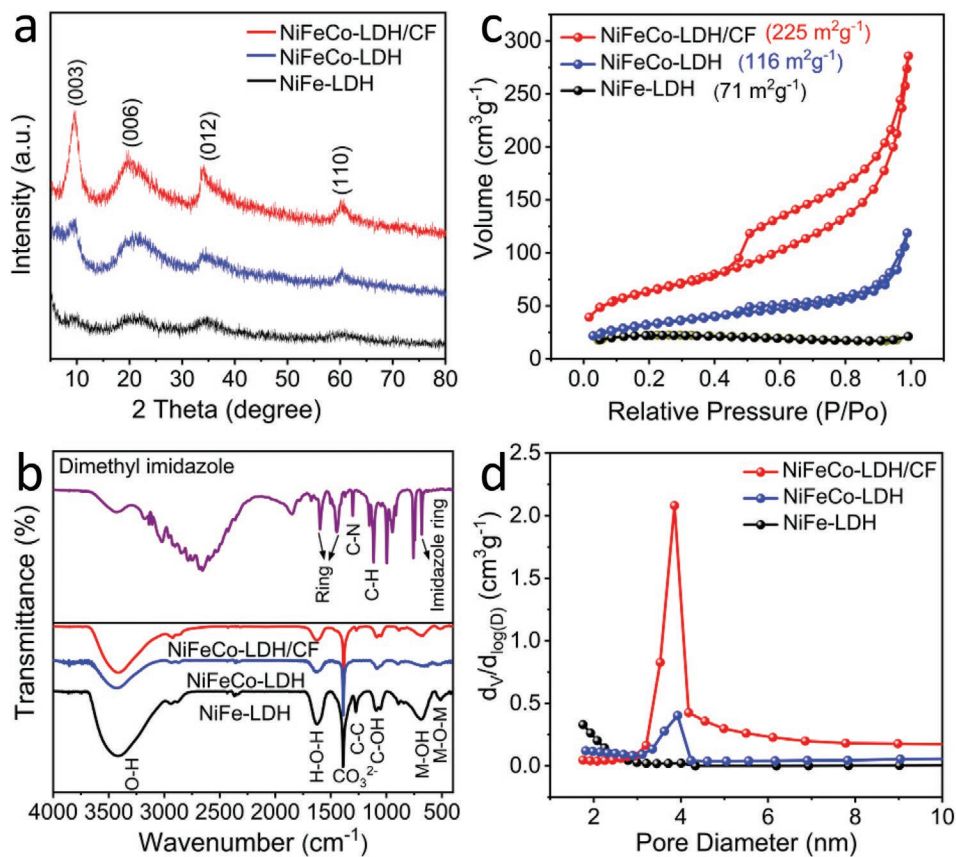
Figure 3. a) XRD patterns of NiFe-LDH, NiFeCo-LDH, and NiFeCo-LDH/CF. b) FT-IR spectra of dimethyl imidazole, NiFeCo-LDH/CF, NiFeCo-LDH, and NiFe-LDH. c) Nitrogen adsorption/desorption isotherms and d) corresponding pore size distribution of NiFe-LDH, NiFeCo-LDH, and NiFeCo-LDH/CF, respectively.

to the electron excitation from 1s to 4p orbital. In general, the average valence of element species is proportional to their edge energy, representing that the element species with higher oxidation state have a higher absorption threshold position.[24] As displayed in Figure 4d, the absorption threshold positions of Ni in the samples are generally proportional to the valence. The threshold position of NiO is the lowest, followed by LiNiO2. Notably, the threshold position of NiFeCo-LDH/CF is extremely close to that of NiO, revealing that the valence of Ni in the sample is Ni (II). Similarly, the threshold position of Fe overlaps with that of α-Fe$_2$O$_3$ (Figure 4e), referring that the existence of Fe(III) valence in the sample. In addition, the threshold position of Co in the sample locates between CoO and Co$_3$O$_4$ (Figure 4f), evidencing the existence of mixed valence of cobalt (Co (II)/Co(III)) in NiFeCo-LDH/CF. The accurate Ni, Fe, and Co valences in these samples are further evaluated from the reference-derived linear regressions (Figure S9a–c, Supporting Information). These analyses are in good agreement with the aforementioned XPS results.

The oscillation amplitude frequencies of the samples are contributed by the vibration between center atom and its neighbor atom. As shown in **Figure 5**a b, the oscillation amplitude frequencies of Ni and Fe between NiFe-LDH and NiFeCo-LDH/CF were similar, indicating that the Ni and Fe coordination environment was independent of CF and Co

incorporation. In addition, the oscillation amplitude frequencies of Co in the NiFeCo-LDH/CF (Figure 5c) were also identical to that of Ni, revealing the substitution of Co atom for partly original Ni atom, without changing the lattice parameter of basic NiFe-LDH. EXAFS for the as synthesized catalysts, providing direct evidence for the local structure and coordination environment, are shown in Figure 5d–f. In terms of Co incorporation, as shown in Figure 5d, the bonding distances of Ni—O and Ni—Ni were unchanged, while the intensity of second shell (Ni—Ni/Ni—Co) increased due to the Co substitution effect.[25] This phenomenon was corresponding to the obvious stabilization of atomic structure in Fe species for NiFeCo-LDH/CF catalyst (Figure 5e). The EXAFS spectra of Co K-edge for NiFeCo-LDH/CF (Figure 5f) shows two coordination peaks which are identical to those of Ni K-edge, also revealing the substitutional doping of Co in the Ni(OH)$_2$ host. Furthermore, the high-spin Fe(III) has much unoccupied state in π-symmetry t$_{2g}$ d-orbitals relative to Ni (II) and Co(II)/Co(III) with all doubly occupied t$_{2g}$ d-orbitals.[26] In general, the stabilization of Fe coordination environment can promote the stronger Ni3d–O2p and Co3d–O2p covalency due to their better, e.g., d-orbital hybridization with oxygen-related adsorbate.[27] On the basis of these results, we concluded that the Co substitution can stabilize the Fe local coordination environment and facilitate the π-symmetry bonding orbital in

**ADVANCED
SCIENCE NEWS**

www.advancedsciencenews.com
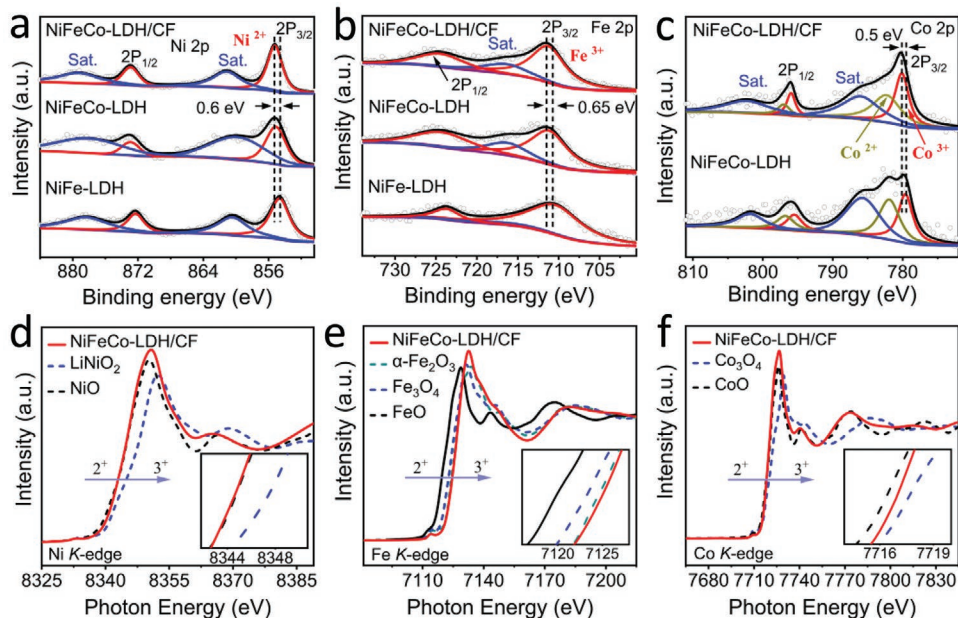
**NANO · MICRO
small**

www.small-journal.com

Figure 4. XPS spectra of a) Ni 2p and b) Fe 2p for NiFeCo-LDH/CF, NiFeCo-LDH, and NiFe-LDH, respectively. c) XPS spectra of Co 2p for NiFeCo-LDH/CF and NiFeCo-LDH. XANES spectra of d) Ni K-edge, e) Fe K-edge, and f) Co K-edge for NiFeCo-LDH/CF.

NiFeCo-LDH/CF catalyst. Hence, the stronger Ni3d–O2p and Co3d–O2p covalency would significantly modify the electronic structures and improve the OER activity for NiFeCo-LDH/CF catalyst. Different from the reported works focusing on improving the electrode performance by rationally designing the electrode structure,[16,28] our work combines rational structure design by using ZIF-67/CF and electronic structure modulation by introducing Co at the same time, both contributing to the superior OER activity.

The electrocatalytic performance of the as-prepared catalysts for OER were investigated using a standard three-electrode system in N_2-saturated 1 M KOH electrolyte with an active material loading of 0.28 mg cm^{-2} on glassy carbon substrate. The performance evaluation is based on the linear sweep voltammetry (LSV) curves recorded on an electrochemical workstation, as shown in **Figure 6**. To make a fair comparison of the effect of different cobalt content on OER property, two control samples of 0.5-NiFeCo-LDH and 2-NiFeCo-LDH were also prepared
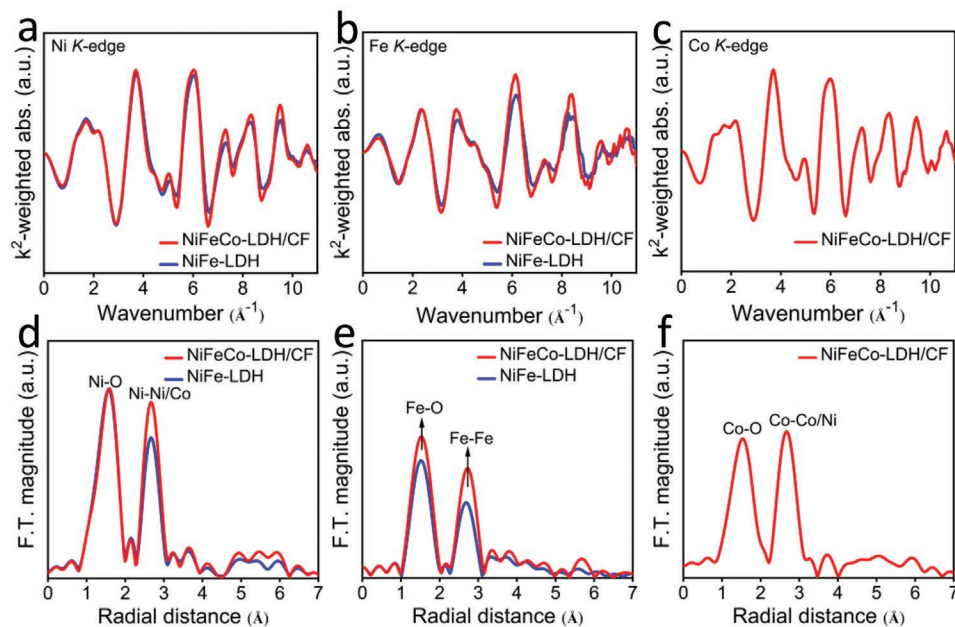

Figure 5. EXAFS oscillation spectra of a) Ni K-edge, b) Fe K-edge, and c) Co K-edge for NiFe-LDH and NiFeCo-LDH/CF, respectively. Fourier transform (FT)–EXAFS spectra of d) Ni K-edge, e) Fe K-edge, and f) Co K-edge of NiFe-LDH and NiFeCo-LDH/CF, respectively.
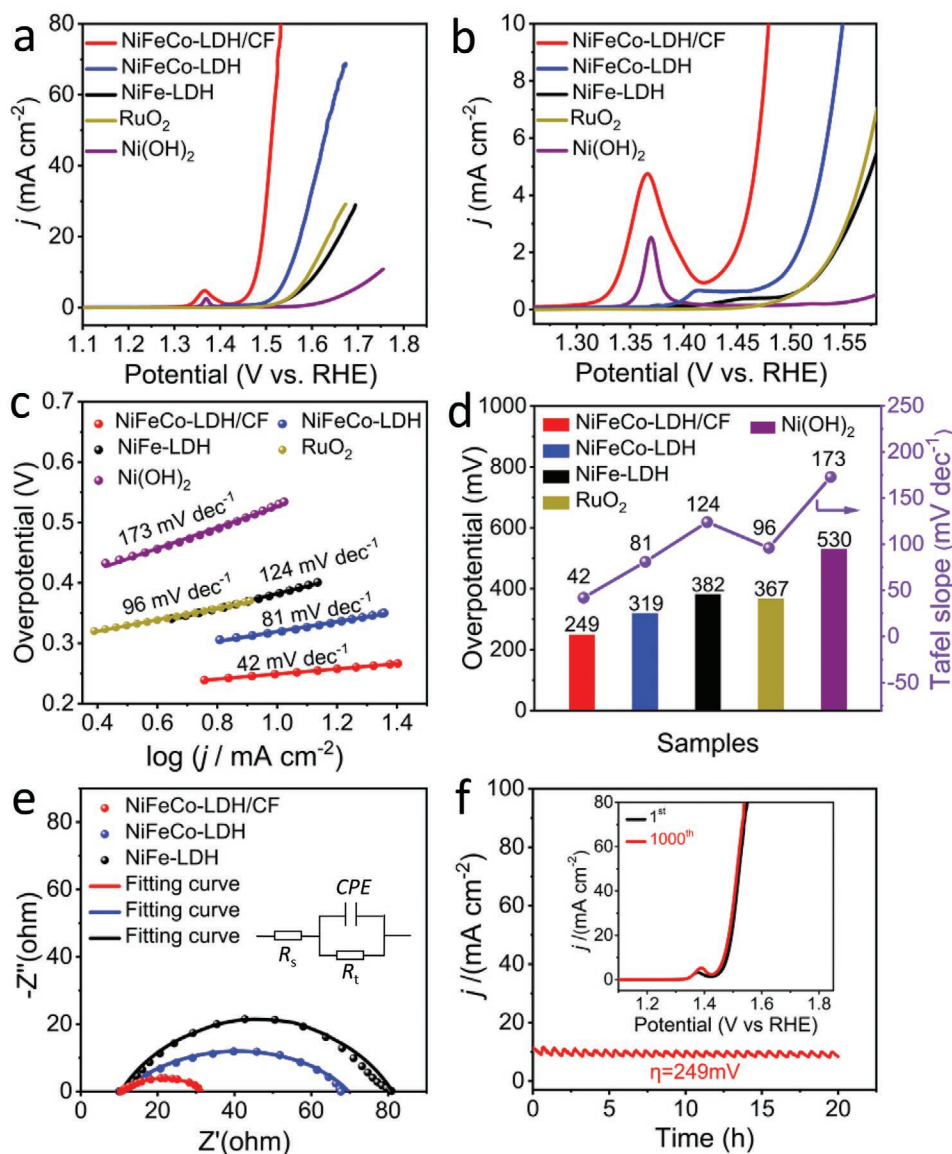
**ADVANCED
SCIENCE NEWS**

www.advancedsciencenews.com

**NANO · MICRO
small**

www.small-journal.com

Figure 6. a) OER polarization curves of $Ni(OH)_2$, RuO_2, NiFe-LDH, NiFeCo-LDH, and NiFeCo-LDH/CF at a scan rate of 5 mV s^{-1} in 1 M KOH electrolyte. b) Enlarged polarization curves showing the oxidation peaks for various samples. c) Corresponding Tafel slopes derived from OER polarization curves for different catalysts. d) Comparison of overpotentials at 10 mA cm^{-2} and Tafel slopes among various catalysts. e) Nyquist plots for NiFe-LDH, NiFeCo-LDH, and NiFeCo-LDH/CF at the overpotential of 320 mV. f) Chronoamperometry measurement for NiFeCo-LDH/CF at overpotential of 249 mV with inset showing LSV curves before and after 1000 CV cycles at a scan rate of 20 mV s^{-1}.

by using half or twofold weight of the ZIF-67 precursor instead of ZIF-67/CF, compared with that used for the preparation of NiFeCo-LDH. As shown in Figure S10 and Table S1 of the Supporting Information, the OER catalytic activity for the catalysts greatly improved when the atomic ratio of Co increased from 8.69% to 16.34%. However, when continuously increased the atomic ratio of Co to 48.77% in the NiFeCo-LDH, slight change for the OER activity can be observed. Taking the cost and yield rate of ZIF-67 into consideration, we consider the synthetic ratio of NiFeCo-LDH as the optimum ratio (using 230 mg ZIF-67). The content of carbon fiber in ZIF-67/CF in relation to OER performance has also been investigated (Figure S11, Supporting Information). It is worth noting that with the incorporation

of CF, a series of NiFeCo-LDH/CFs remarkably outperform the bare NiFeCo-LDH, which could be owing to the structural features, including the largely exposed active surface sites and facilitated charge transfer pathway ensured by CF. With the increase of the CF content, the catalytic activity of NiFeCo-LDH/CF increases and reaches a maximum value. However, further increasing the CF ratio results in performance degradation, which may be caused by the poor OER catalytic activity of CF itself. The representative NiFeCo-LDH/CF with an original CF content of 7.5% in ZIF-67/CF precursor shows the best OER activity among a series of catalysts with various carbon fiber contents. Figure 6a presents the LSV curves for a comparing examination of NiFeCo-LDH/CF, NiFeCo-LDH, NiFe-LDH,

ADVANCED
SCIENCE NEWS
www.advancedsciencenews.com

NANO · MICRO
small
www.small-journal.com

and Ni(OH)$_2$, revealing distinguished OER performance of NiFeCo-LDH/CF and NiFeCo-LDH than NiFe-LDH, as well as the benchmark catalyst RuO$_2$. Partially enlarged region of OER polarization curves in Figure 6a of these samples are shown in Figure 6b. The anodic peak of Ni(OH)$_2$ at 1.38V (vs RHE) is due to the oxidation of Ni^{2+} to Ni^{3+}. The Ni(OH)$_2$ sample itself as a reference shows minimal OER activity as it is shown in higher potential region with nearly no OER current response. The NiFeCo-LDH/CF and NiFeCo-LDH demonstrate superior OER performance than that of NiFe-LDH evidenced by the lower Ni^{2+} to Ni^{3+} oxidation potentials and OER onset potentials, with NiFeCo-LDH/CF being more prominent. This results indicate that Co can promote oxidation of Ni^{2+} to Ni^{3+} forming NiOOH at lower potential.[29] On the one hand, the improvement of OER performance for NiFeCo-LDH/CF may be attributed to the activation of more conductive NiOOH phase by the charge transfer effect of Co. On the other hand, the conductively tubular frizzy structure established by CF can offer the sufficient supply of electron for NiFeCo-LDH/CF during the electrocatalytic OER process. In order to better understand the electrochemical reaction kinetics, corresponding Tafel slopes derived from LSV curves of the catalysts were further analyzed in Figure 6c. Among all the catalysts, NiFeCo-LDH/CF displays a smaller Tafel slope of 42 mV dec^{-1}, while those of NiFeCo-LDH and NiFe-LDH are 81 and 124 mV dec^{-1}, respectively, indicating a possible change in the reaction control step for NiFeCo-LDH/CF. The small value of Tafel slope, an important intrinsic trait of electrocatalyst, means a high achievable current at a given overpotential. The comparison of overpotential at current density of 10 mA cm^{-2} and Tafel slope among the various catalysts are presented in Figure 6d. It can be seen that NiFeCo-LDH/CF exhibits the lowest overpotential (249 mV at $j = 10$ mA cm^{-2}) and the same trend of Tafel slopes for the series catalysts, which can be attributed to the optimized electronic structure permitting fast charge transfer and benefiting adsorption/desorption for oxygenated species.[17b,30] Furthermore, partial electronic redistribution among Ni, Fe, and Co by the bridging O^{2-} at the interface of the catalysts can further improve the adsorption/desorption character of oxygenated species, thus enhancing the electrocatalytic kinetics for OER. More comparison for OER activities with other nickel, iron, and/or cobalt-based catalysts in recently reported literatures was also summarized in Table S2 of the Supporting Information. It is seen that NiFeCo-LDH/CF possesses prominent OER catalytic properties and even can be comparable or superior to other reported electrocatalysts. Furthermore, to authenticate the real active sites in NiFeCo-LDH/CF catalyst, LSV curves for other series of related LDH/CF catalysts were explored as well. As shown in Figure S12 of the Supporting Information, NiFeCo-LDH/CF exceedingly outperforms the FeCo-LDH/CF, NiCo-LDH/CF, and Co-LDH/CF catalysts, which indicate that only the presence of three Ni, Fe, and Co components and their synergistic effect can ensure the extraordinary OER activity of NiFeCo-LDH/CF.

The electrochemically active surface areas of the synthesized catalysts were estimated by their double-layer capacitances (C_{dl}) according to the cyclic voltammogram (CV) measurement. The detailed CV profiles measured in the non-Faradaic potential regions at various scan rates are presented in Figure S13a,c,e of the Supporting Information and the derived C_{dl} plots are shown

in Figure S13b,d,f of the Supporting Information. NiFeCo-LDH/CF owns the largest C_{dl} of 0.71 mF cm^{-2} than those of NiFe-LDH (0.12 mF cm^{-2}) and NiFeCo-LDH (0.28 mF cm^{-2}), indicating that NiFeCo-LDH/CF has more porosity with higher specific surface area, in agreement with the BET results. To gain further insight into the superior OER reaction kinetics of NiFeCo-LDH/CF, electrochemical impedance spectroscopies of all the NiFe-based catalysts were measured at an applied overpotential of 320 mV from 100 kHz to 0.01 Hz and the Nyquist plots and fitting equivalent circuit model are given in Figure 6e. The Nyquist plots show depressed semicircles, indicating the porous nature of the catalyst materials represented by the constant phase element in the equivalent circuit model. Compared with those of NiFe-LDH and NiFeCo-LDH, the charge transfer resistance (R_{ct}) value for NiFeCo-LDH/CF is smaller. The R_{ct} results obtained at an overpotential of 320 mV in 1 M KOH are 23.5, 63.3, and 72.9 Ω cm^{-2} for NiFeCo-LDH/CF and NiFeCo-LDH and NiFe-LDH, respectively. The outstanding faster charge transfer and lower electronic resistance properties of NiFeCo-LDH/CF are highly consistent with the result of the Tafel slope. These results indicate that the introduction of CF and Co in NiFeCo-LDH/CF increases the electronic conductivity and accelerates the charge transfer rate during the OER process.[30,31] Furthermore, as shown in Figure 6f, the evaluation of NiFeCo-LDH/CF stability was carried out by chronoamperometry measurement. Compared with NiFe-LDH and NiFeCo-LDH (Figure S14, Supporting Information), the NiFeCo-LDH/CF catalyst exhibits outstanding stability at an overpotential of 249 mV, which displays only a negligible degradation in current density after the long electrolysis of 20 h. Meanwhile, the long cycle LSV curves were presented in the inset in Figure 6f as well. It shows that the LSV profiles are almost unchanged after 1000 CV cycles, which further proves that NiFeCo-LDH/CF has advantageous durability. The SEM images of NiFeCo-LDH/CF after OER polarization at 249 mV overpotential for 20 h are shown in Figure S15 of the Supporting Information. It can be clearly seen that NiFeCo-LDH/CF basically retains the integrated morphology after the OER test. Besides, the XPS patterns for NiFeCo-LDH/CF after the long-term OER measurement (Figure S16, Supporting Information) are shown to be similar with those before the polarization (Figure 4), except that part of Ni^{2+} was oxidized into Ni^{3+} during the OER procedure. Furthermore, XANES spectra of Ni K-edge, Fe K-edge, and Co K-edge for NiFeCo-LDH/CF before and after OER also reveal the robustness of NiFeCo-LDH/CF for OER electrocatalysis (Figure S17, Supporting Information). In general, all these results further suggest the outstanding stability of NiFeCo-LDH/CF.

3. Conclusions

In summary, we elaborately developed a facile strategy to fabricate a 3D composite with frizzy edge-rich NiFeCo-LDH nanosheets on CF. EXAFS shows the Co substitution for partly original Ni atom can stabilize the Fe local coordination environment and facilitate the π-symmetry bonding orbital in the NiFeCo-LDH catalyst. Hence, the stronger Ni3d–O2p and Co3d-O2p covalency would significantly modify the electronic

structures and improve the OER activity for the NiFeCo-LDH catalyst. Besides, with the help of ZIF-67/CF, the frizzy ultrathin nanosheets of NiFeCo-LDH growing on carbon fiber could completely expose its active sites by diminishing the thickness and increasing the specific surface area. Moreover, the sufficient supply of electron to NiFeCo-LDH/CF could be ensured by the conductively tubular frizzy structure incorporated with CF during the electrocatalytic OER processes. The resulting NiFeCo-LDH/CF exhibits superior OER performance than that of previous benchmarked NiFe-LDH in alkaline electrolyte. As a result, NiFeCo-LDH/CF exhibits a superior OER activity with an onset potential of 1.43 V versus RHE, an overpotential of 249 mV at 10 mA cm^{-1} as well as robust stability over 20 h. After an insightful understanding into the outstanding OER performance, we expect that this work may open up a new strategy to design and fabricate more active and stable electrocatalysts for various energy storages and conversions.

Supporting Information

Supporting Information is available from the Wiley Online Library or from the author.

Acknowledgements

Conflict of Interest

The authors declare no conflict of interest.

Keywords

[1] a) A. Kudo, Y. Miseki, *Chem. Soc. Rev.* **2009**, *38*, 253; b) T. R. Cook, D. K. Dogutan, S. Y. Reece, Y. Surendranath, T. S. Teets, D. G. Nocera, *Chem. Rev.* **2010**, *110*, 6474.

[2] R. D. Smith, M. S. Prévot, R. D. Fagan, Z. Zhang, P. A. Sedach, M. K. J. Siu, S. Trudel, C. P. Berlinguette, *Science* **2013**, *340*, 60.

[3] Y. Lee, J. Suntivich, K. J. May, E. E. Perry, Y. Shao-Horn, *J. Phys. Chem. Lett.* **2012**, *3*, 399.

[4] G. Chen, Y. P. Zhu, H. M. Chen, Z. W. Hu, S. F. Hung, N. N. Ma, J. Dai, H. J. Lin, C. T. Chen, W. Zhou, Z. P. Shao, *Adv. Mater.* **2019**, *31*, 1900883.

[5] a) X. Wang, L. Yu, B. Y. Guan, S. Song, X. W. Lou, *Adv. Mater.* **2018**, *30*, 1801211; b) F. Song, L. Bai, A. Moysiadou, S. Lee, C. Hu, L. Liardet, X. Hu, *J. Am. Chem. Soc.* **2018**, *140*, 7748.

[6] a) Y. Q. Zhang, B. O. Yang, J. Xu, G. C. Jia, S. Chen, R. S. Rawat, H. J. Fan, *Angew. Chem., Int. Ed.* **2016**, *55*, 8670; b) Y. Fan, S. Ida, A. Staykov, T. Akbay, H. Hagiwara, J. Matsuda, K. Kaneko, T. Ishihara, *Small* **2017**, *13*, 1700099.

[7] Y. J. Tang, C. H. Liu, W. Huang, X. L. Wang, L. Z. Dong, S. L. Li, Y. Q. Lan, *ACS Appl. Mater. Interfaces* **2017**, *9*, 16977.

[8] a) K. Wan, J. S. Luo, C. Zhou, T. Zhang, J. Arbiol, X. H. Lu, B. W. Mao, X. Zhang, J. Fransaer, *Adv. Funct. Mater.* **2019**, *29*, 1900315; b) Y. Wu, F. Li, W. Chen, Q. Xiang, Y. Ma, H. Zhu, P. Tao, C. Song, W. Shang, T. Deng, J. Wu, *Adv. Mater.* **2018**, *30*, 1803151; c) H. Wang, Y. Cao, C. Sun, G. Zou, J. Huang, X. Kuai, J. Zhao, L. Gao, *ChemSusChem* **2017**, *10*, 3540.

[9] a) Z. Cai, D. Zhou, M. Wang, S. M. Bak, Y. Wu, Z. Wu, Y. Tian, X. Xiong, Y. Li, W. Liu, S. Siahrostami, Y. Kuang, X. Q. Yang, H. Duan, Z. Feng, H. Wang, X. Sun, *Angew. Chem., Int. Ed.* **2018**, *57*, 9392; b) H. Zhang, X. Li, A. Hähnel, V. Naumann, C. Lin, S. Azimi, S. L. Schweizer, A. W. Maijenburg, R. B. Wehrspohn, *Adv. Funct. Mater.* **2018**, *28*, 1706847; c) L. Yu, J. F. Yang, B. Y. Guan, Y. Lu, X. W. Lou, *Angew. Chem., Int. Ed.* **2018**, *57*, 172; d) C. Luan, G. Liu, Y. Liu, L. Yu, Y. Wang, Y. Xiao, H. Qiao, X. Dai, X. Zhang, *ACS Nano* **2018**, *12*, 3875; e) A. M. P. Sakita, E. Vallés, R. D. Noce, A. V. Benedetti, *Appl. Surf. Sci.* **2018**, *447*, 107.

[10] a) F. Dionigi, P. Strasser, *Adv. Energy Mater.* **2016**, *6*, 1600621; b) J. Chen, F. Zheng, S.-J. Zhang, A. Fisher, Y. Zhou, Z. Wang, Y. Li, B.-B. Xu, J.-T. Li, S.-G. Sun, *ACS Catal.* **2018**, *8*, 11342; c) K. Zhu, H. Liu, M. Li, X. Li, J. Wang, X. Zhu, W. Yang, *J. Mater. Chem. A* **2017**, *5*, 7753; d) X. Zhang, Y. Zhao, Y. Zhao, R. Shi, G. I. N. Waterhouse, T. Zhang, *Adv. Energy Mater.* **2019**, *9*, 1900881; e) J. Zhang, J. Liu, L. Xi, Y. Yu, N. Chen, S. Sun, W. Wang, K. M. Lange, B. Zhang, *J. Am. Chem. Soc.* **2018**, *140*, 3876; f) Q. He, H. Xie, Z. U. Rehman, C. D. Wang, P. Wan, H. L. Jiang, W. S. Chu, L. Song, *ACS Energy Lett.* **2018**, *3*, 861; g) J. Jiang, F. Sun, S. Zhou, W. Hu, H. Zhang, J. Dong, Z. Jiang, J. Zhao, J. Li, W. Yan, M. Wang, *Nat. Commun.* **2018**, *9*, 2885; h) Y. Lin, Y. Li, Q. Lan, X.-J. Lv, S. Liu, D. Liu, W. Hu, *J. Alloys Compd.* **2018**, *744*, 347.

[11] L. Trotochaud, S. L. Young, J. K. Ranney, S. W. Boettcher, *J. Am. Chem. Soc.* **2014**, *136*, 6744.

[12] a) J. G. Li, H. Sun, L. Lv, Z. Li, X. Ao, C. Xu, Y. Li, C. Wang, *ACS Appl. Mater. Interfaces* **2019**, *11*, 8106; b) P. Liu, D. Gao, W. Xiao, L. Ma, K. Sun, P. Xi, D. Xue, J. Wang, *Adv. Funct. Mater.* **2018**, *28*, 1706928.

[13] a) J. Yang, F. Zhang, H. Lu, X. Hong, H. Jiang, Y. Wu, Y. Li, *Angew. Chem., Int. Ed.* **2015**, *54*, 10889; b) W. Sun, X. Zhai, L. Zhao, *Chem. Eng. J.* **2016**, *289*, 59; c) Y. Pan, K. Sun, S. Liu, X. Cao, K. Wu, W. C. Cheong, Z. Chen, Y. Wang, Y. Li, Y. Liu, D. Wang, Q. Peng, C. Chen, Y. Li, *J. Am. Chem. Soc.* **2018**, *140*, 2610; d) Y.-N. Liu, H.-T. Wang, X.-H. Kang, Y.-F. Wang, S.-Y. Yang, S.-W. Bian, *J. Power Sources* **2018**, *402*, 413.

[14] R. Banerjee, A. Phan, B. Wang, C. Knobler, H. Furukawa, M. O'Keeffe, O. M. Yaghi, *Science* **2008**, *319*, 939.

[15] Z. Jiang, Z. Li, Z. Qin, H. Sun, X. Jiao, D. Chen, *Nanoscale* **2013**, *5*, 11770.

[16] C. Liang, P. Zou, A. Nairan, Y. Zhang, J. Liu, K. Liu, S. Hu, F. Kang, H. J. Fan, C. Yang, *Energy Environ. Sci.* **2020**, *13*, 86.

[17] a) M. Gong, Y. Li, H. Wang, Y. Liang, J. Z. Wu, J. Zhou, J. Wang, T. Regier, F. Wei, H. Dai, *J. Am. Chem. Soc.* **2013**, *135*, 8452; b) Y. Liu, S. Liu, Y. Wang, Q. Zhang, L. Gu, S. Zhao, D. Xu, Y. Li, J. Bao, Z. Dai, *J. Am. Chem. Soc.* **2018**, *140*, 2731; c) Y. Wang, D. Yan, S. El Hankari, Y. Zou, S. Wang, *Adv. Sci.* **2018**, *5*, 1800064.

[18] S.-H. Bae, J.-E. Kim, H. Randriamahazaka, S.-Y. Moon, J.-Y. Park, I.-K. Oh, *Adv. Energy Mater.* **2017**, *7*, 1601492.

[19] X. Zhu, C. Tang, H.-F. Wang, Q. Zhang, C. Yang, F. Wei, *J. Mater. Chem. A* **2015**, *3*, 24540.

[20] a) M. A. U. J. M. Fernandez, F. M. Labajos, V. Rives, *J. Mater. Chem.* **1998**, *8*, 2507; b) M. Wei, X. Xu, J. He, Q. Yuan, G. Rao, D. G. Evans, M. Pu, L. Yang, *J. Phys. Chem. Sol.* **2006**, *67*, 1469.

[21] L. Chen, B. Sun, X. Wang, F. Qiao, S. Ai, *J. Mater. Chem. B* **2013**, *1*, 2268.

[22] L. Jiao, G. Wan, R. Zhang, H. Zhou, S. H. Yu, H. L. Jiang, *Angew. Chem., Int. Ed.* **2018**, *57*, 8525.

[23] K. Fan, H. Chen, Y. Ji, H. Huang, P. M. Claesson, Q. Daniel, B. Philippe, H. Rensmo, F. Li, Y. Luo, L. Sun, *Nat. Commun.* **2016**, *7*, 11981.

[24] a) P. S. Li, M. Y. Wang, X. X. Duan, L. R. Zheng, X. P. Cheng, Y. F. Zhang, Y. Kuang, Y. P. Li, Q. Ma, Z. X. Feng, W. Liu, X. M. Sun, *Nat. Commun.* **2019**, *10*, 1711; b) H. Wang, X. Xiao, S. Liu, C. L. Chiang, X. Kuai, C. K. Peng, Y. C. Lin, X. Meng, J. Zhao, J. Choi, Y. G. Lin, J. M. Lee, L. Gao, *J. Am. Chem. Soc.* **2019**, *141*, 18578.

[25] S. H. Ye, Z. X. Shi, J. X. Feng, Y. X. Tong, G. R. Li, *Angew. Chem., Int. Ed.* **2018**, *57*, 2672.

[26] J. Y. Chen, L. Dang, H. Liang, W. Bi, J. B. Gerken, S. Jin, E. E. Alp, S. S. Stahl, *J. Am. Chem. Soc.* **2015**, *137*, 15090.

[27] a) J. K. Nørskov, F. Abild-Pedersen, F. Studt, T. Bligaard, *Proc. Natl. Acad. Sci. USA* **2011**, *108*, 937; b) H. Shin, H. Xiao, W. A. Goddard III, *J. Am. Chem. Soc.* **2018**, *140*, 6745.

[28] L. Yu, H. Zhou, J. Sun, I. K. Mishra, D. Luo, F. Yu, Y. Yu, S. Chen, Z. Ren, *J. Mater. Chem. A* **2018**, *6*, 13619.

[29] M. K. Bates, Q. Jia, H. Doan, W. Liang, S. Mukerjee, *ACS Catal.* **2016**, *6*, 155.

[30] H. Li, Q. Zhou, F. Liu, W. Zhang, Z. Tan, H. Zhou, Z. Huang, S. Jiao, Y. Kuang, *Appl. Catal., B* **2019**, *255*, 117755.

[31] M. S. Burke, M. G. Kast, L. Trotochaud, A. M. Smith, S. W. Boettcher, *J. Am. Chem. Soc.* **2015**, *137*, 3638.